Applied Physics A (2025) 131:798
https://doi.org/10.1007/s00339-025-08838-8

Applied Physics A
Materials Science & Processing

Wear behavior optimization of friction stir processed Mg-TiC composites through response surface methodology

Avtar Singh[1] · Saurabh Chaitanya[2] · Sachin Mohal[2] · Neeraj Kamboj[1] · Md Irfanul Haque Siddiqui[3] · Intesaaf Ashraf[4]

Received: 5 March 2025 / Accepted: 27 July 2025 / Published online: 24 September 2025

Abstract
This work examined the behavior of Mg-TiC composites fabricated using a stir casting process followed by a single-pass friction stir process (FSP). Morphological analysis revealed a uniform distribution of TiC reinforcement, effectively mitigating the reinforcement agglomeration issues. The composites processed at 1400 rpm (FSP) exhibited a 26% improvement in microhardness compared to cast Mg-TiC composites and 60% compared to pure Mg processed at the same parameters. The wear behavior was optimized using response surface methodology (RSM), considering load, sliding distance and sliding velocity as key parameters. The results exhibit an increase in the volumetric wear rate. The morphological examination of worn surfaces using scanning electron microscope (SEM), highlighted abrasive, adhesive, and oxidative wear mechanisms. The findings reveal the refined microstructure, enhanced microhardness, and superior wear behaviour of the processed magnesium matrix composites.

Keywords Magnesium matrix composite · TiC · Friction stir processing · RSM · Wear behavior

1 Introduction

Magnesium matrix based composite materials are conquering status of a structural material in automobile segment to reduce the pollution [1]. Magnesium has good specific strength, machinability, castability property. Also, Mg has low density and lighter as compared to aluminum and steel respectively. However, poor wear resistance and hardness confine its usage [2]. To overcome these limitations, various reinforcements like titanium carbide (TiC) [3], silicon carbide (SiC) [4], Boron Carbide (B_4C) [5], alumina (Al_2O_3) [6], zirconium oxide (ZrO_2) [7], can be added to magnesium matrix material to attain good wear resistance, strength and hardness. Magnesium metal matrix composites (MMMC) have shown noteworthy enhancement in mechanical properties as compared to monolithic magnesium. MMMC can be produced by various processes, like stir casting [8], powder metallurgy [9], and stir squeeze casting [10]. Stir casting method is considered as cost-effective technique to produce composites as equated to their related processes [11]. Although some limits of stir casting process viz. reinforcements cluster, particle condensed sections and particle free sections were spotted in composites [12]. These defects can be reduced by various practices such as forging and extrusion that might solve the above-mentioned problems; though, the procedure is laborious. These defects can abolish by using FSP, which improves mechanical properties of composites also [13]. Friction stir processing is the resultant of friction stir welding process and widely used to produce surface composites [14]. FSP is a solid-state process which does not melt the work piece. The specifically designed cylindrical tool consists of a pin and a shoulder is used in FSP. In friction stir

Avtar Singh and Saurabh Chaitanya equally contributed to this article.

✉ Intesaaf Ashraf
intesaaf.ashraf@ucl.ac.uk

Sachin Mohal
sachinmohal13@gmail.com

[1] Chandigarh Group of Colleges-COE, Landran, Mohali 140307, Punjab, India

[2] Chandigarh Engineering College-CGC, Landran, Mohali 140307, Punjab, India

[3] Department of Mechanical Engineering, College of Engineering, King Saud University, Riyadh 12372, Saudi Arabia

[4] Mechanical Engineering Department, University College London, London WC1E 7J, UK

processing, heat is generated by rubbing of rotating shoulder which softens the material and pin plunged into specimen triggered the mechanical stirring. The material under the processed region go through the extreme plastic deformation which yields recrystallized fine grain structure [15].

Various studies have undertaken to study the effects of FSP on microstructure and mechanical properties of processed specimens. Zykova et al. [16] showed the improved grains and dissolution of second phase particles, which refined the grain size in the matrix and eliminates the porosity by FSP. FSP effectively removed macroscopic and microscopic defects (void and porosity) existing in the castings [17]. Iwaszko and Kudła [18] investigated the microstructure of AZ91 magnesium alloy produced by FSP, which showed grain refinement and equiaxed recrystallized grains in the stirrer area. In FSP rotational speed of tool played a vital role in producing fine grain structure along with defect-free nugget zone and enhanced mechanical properties [19]. Ahmadkhaniha et al. [20] reported that AZ91/Al_2O_3 nanocomposites fabricated by FSP showed improved hardness and reduced grain size at low rotational speed of FSP tool. Ready composite exhibits enhanced wear resistance due to existence of Al_2O_3 nano particles and also due to FSP. Shang et al. [21] investigated the use of stiffer and harder reinforcement, which produced the composites with enhanced strength and wear resistance. Vikas et al. [22] examined the effect of FSP on metallurgical properties of AZ91D, which showed homogenous dispersal of reinforcement particles and refined grain size. The granular structure obtained by the multi pass FSP may have contributed to the specimens' increased ultimate tensile strength. FSP as secondary process on as cast AA5083-SiC nanocomposites and found the refined microstructure and improved strength of composite [23]. Uniformly distributed reinforced particles were obtained in AA5083 alloy surface composites processed by FSP [24]. Single pass method of FSP helped to improve the hardness of processed AZ31 Magnesium alloy [25].

Titanium carbide (TiC) is considered as good reinforcement material due to high hardness, and wear resistance [26, 27]. Mohammad and Kamran [28] studied that magnesium/TiC surface composites formed by FSP showed noteworthy refinement in microstructure and enhanced hardness. The average hardness increased from 50 Vickers to 79 Vickers. Balakrishnan et al. [29] studied the microstructure of AZ91/TiC based surface composites produced by single pass FSP. Investigation determined that TiC particle evenly dispersed in the matrix material without any bunch formation. Singh et al. [30] made-up pure Mg surface composite with the help of FSP, reinforced with TiC. Wear characteristics of fabricated composites have been studied through pin on disk setup, which showed improved wear resistance due to development of better grain structure and existence of fine TiC particles.

The above studies concluded that FSP is worthwhile process, which improves strength, ductility, hardness, wear resistance, mostly refine the microstructure of composite materials. Above investigations initiate that there are minimal studies on optimization of wear behavior of cast Mg-TiC composites processed by FSP. In this study, specimen of pure Mg was similarly processed by FSP for comparison with cast Mg-TiC composite. RSM is a statistical tool that allows for the optimization of process constraints by creating mathematical models and analyzing the connections between input variables and responses [31, 32]. This method allows researchers to study the effects of input process parameters on output responses while optimizing the desired results [33–35]. In the present work, effects of FSP on microstructure, mechanical properties, and wear behavior of as cast composites are studied. Moreover, RSM has been applied on FSPd Mg-TiC composite to study the effect of input parameters on volumetric wear rate.

2 Experimental process

2.1 Materials and preparation

Stir casting route was employed to fabricate the cast composite, pure Mg (matrix material) and TiC powder (reinforced material) were selected in the current study, as described by Singh and Bala [36]. The TiC reinforcement 10% w. was added to Mg matrix melt. The mild steel mold of 80 × 80 × 80 mm was used to pour the melt to prepare composite. The 80 × 80 × 10 mm size plates were cut by wire cut electric discharge machine (EDM) from cast sample for FSP. A CNC vertical milling machine (Make: ACE; 300) utilized to accomplish the FSP wherein as-cast Mg-TiC plates were gripped with fixture on the machine bed. An FSP stainless steel tool having shoulder diameter of 16 mm, pin diameter of 4.5 mm and depth of 4 mm was used to process the samples. FSP was performed at a speed of 30 mm/min and three rotational speeds of 1200, 1400 and 1600 rpm, respectively. Specimens were designated according to rpm of tool, friction stir processed (FSPd) specimens of Mg-TiC composite are designated as FSP 2, FSP 3 and FSP 4 for 1200, 1400 and 1600 rpm respectively. Pure Mg specimen were also friction stir processed for comparison of results. Pure Mg friction stir processed specimen at 1400 rpm is designated as FSP 1. Single pass method of FSP was used to fabricate specimens. The surface textures of FSPd Mg-TiC composites are presented in Fig. 1.

2.2 Microstructure study

Optical microscope and SEM (JEOL, USA) were used to carry out metallographic examinations of the FSPd and

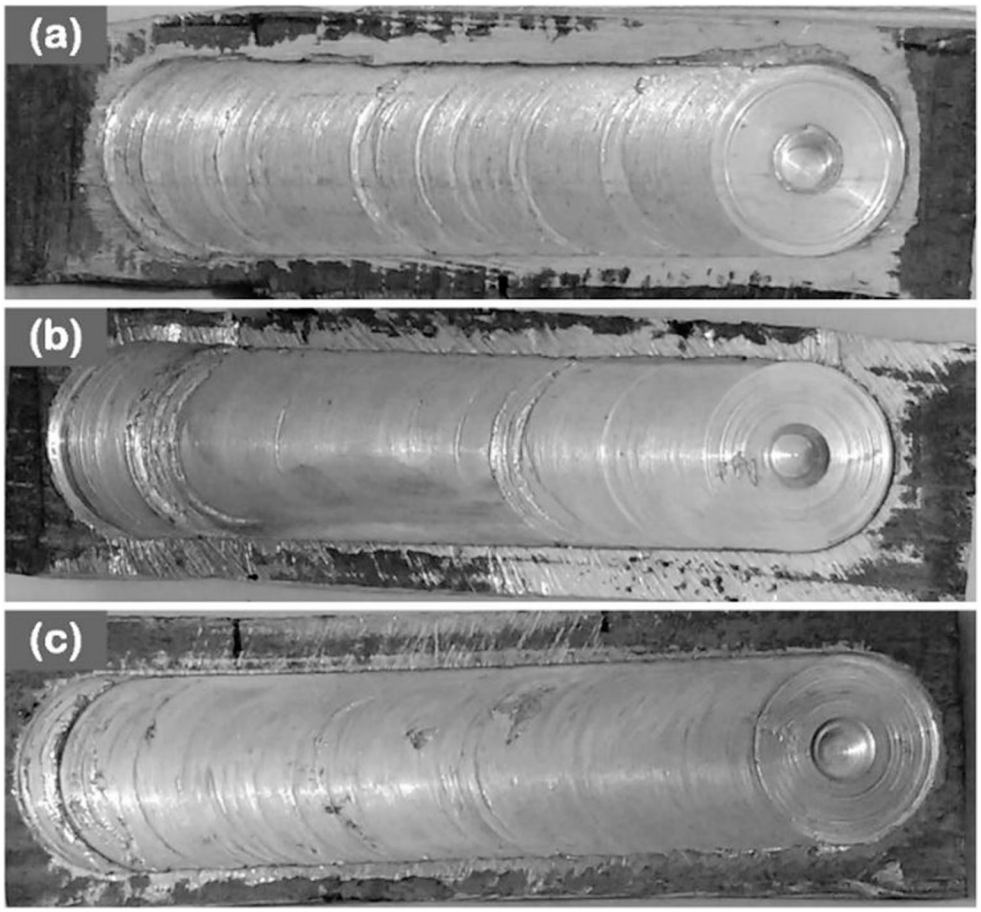

Fig. 1 Macrographs of surface texture FSPd Mg-TiC specimens at (**a**) 1200 (**b**) 1400 and (**c**) 1600 rpm

as-cast samples. The samples were cut by using wire EDM in size of 20 × 20 × 5 mm. The samples were ground with emery papers varying in mesh size up to 3000, polished with alumina powder by using standard procedure of polishing. The etched solution containing distilled H_2O, acetic acid, ethylene glycol and HNO_3 was used for 3–5 s for microstructure study.

2.3 Mechanical properties

Microhardness test was done on FSPd and cast specimens with the help of Vickers microhardness testing machine. For microhardness, the 20 × 20 × 5 mm size samples were polished with different grit size emery paper (400–3000) and with polishing machine (2 disc) of Chennai Metco Pvt. Ltd. A load of 0.05 kg was applied with a hold time of 10 s. For validation of results average of 6 hardness values were booked per sample.

2.4 Wear test

Wear tests were conducted on the pin on disk machine (FRICTION MONITOR-TR 20) furnished by DUCOM Instruments. Rotating disk of EN31 alloy steel was used for wear. The specimens having square dimensions of 5 × 5 mm were cut using wire EDM. All the wear specimens were polished using silicon carbide emery papers upto 1000 grit size, and cleaned with the acetone. Sliding speed of 1 m/s and five loads 5 N, 10 N, 15 N, 20 N, and 25 N were used for wear test. Wear tests were performed 3 times for the conformability of results [36]. An electronic weighing balance equipment with a resolution of 0.001 g was used to weigh the specimens following each test in order to calculate the weight loss. Acetone was used to clean the surface of the steel disk prior to wear test initiation. SEM analysis was done to observe worn surfaces of processed samples.

3 Results and discussion

3.1 Microstructure analysis

The microstructure of cast Mg-TiC composite represented in Fig. 2 (a), which showed clustering of particles at some areas of composite. FSP method assisted in noteworthy refinement of microstructure owed to recrystallization, redistribution of reinforced particles and elimination of clustering of particles. The stirring of tool helped to crash the

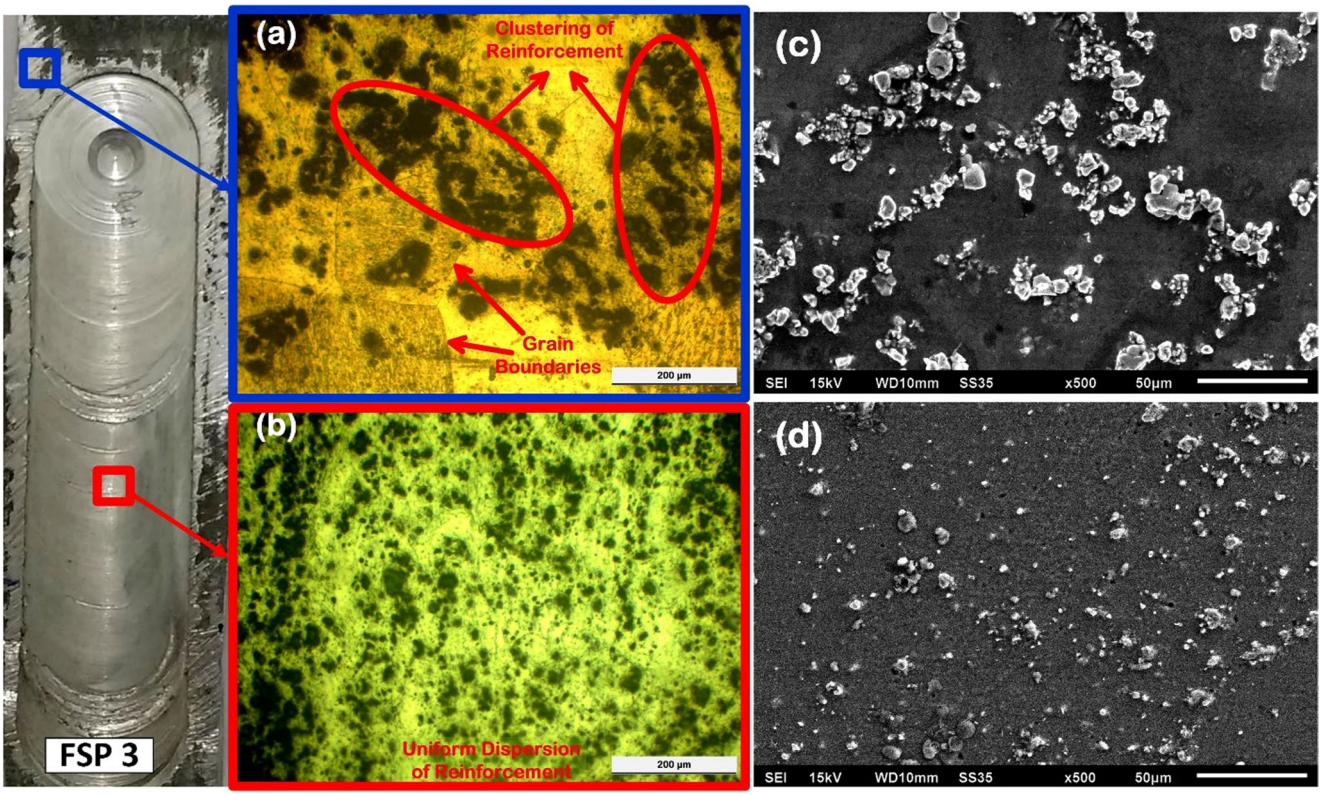

Fig. 2 Optical microstructure and SEM of cast Mg-TiC (**a**, **c**) and FSPd Mg-TiC Composite (**b**, **d**), respectively

clustering locations. Figure 2 (b) has shown sufficient refine grains and uniform dispersal of reinforced particles after the FSP. Processed specimen showed refined grain structure as equated to cast Mg-TiC composites. The improved grain structure and even distribution of particles might be accredited to existence of severe deformation in stirrer zone as stirring action of tool, produced higher frictional heat and leads to redistribution of particles during stirring. FSP was applied to fabricate Al/TiC composite and results showed refined grain structure and improved microhardness as compared to parent material [37]. The existence of hard reinforced TiC particles and plastic deformation induced during FSP aided to refine grain that might be accredited to pining effect of the refined particles and the occurrence of dynamic recrystallization throughout plastic deformation. The present results about the fine-grained microstructure owed to dynamic recrystallization with even distribution of particles in friction stir composites are in arrangement with the studies done by many investigators for magnesium-based composites and alloys as discussed.

SEM micrograph represents that the TiC particles are distributed over the whole area, but some clustering of particles has also been seen at some locations as presented in Fig. 2 (c). SEM micrograph of nugget zone of FSP 3 specimen has been shown in Fig. 2 (d). The SEM images showed that the FSP processed specimen contained very refined and evenly distributed particles of reinforcement. The rotational movement of tool pin plunged in specimen helped to break particles and hence evenly distributed the particles [38]. The particles of TiC got broken and converted into spherical form of fine and medium sized particles that happened owing to stirring of the tool [39]. The evenly distributed refined particles of TiC in FSPd composite might be accredited to the plastic deformations that arise during FSP. Single and double pass FSP to fabricate AA5083/Al_2O_3 composite, which showed refined microstructure and uniform distribution of reinforced material [40]. Good bonding of TiC particles has been observed in SEM micrograph. X-ray mapping of FSPd Mg-TiC composite indicates the elements present in the surface of FSPd composite. Figure 3 evidently shows the existence of Mg, Ti and C elements.

3.2 Mechanical characteristics

Hardness is the most important mechanical characteristic, which resist indentation and abrasion of the materials. Vickers microhardness of Mg-TiC cast composite, pure Mg and FSPd specimens has been presented in Fig. 4, which showed microhardness of the specimens increased considerably after the FSP. Figure 4 represents the microhardness

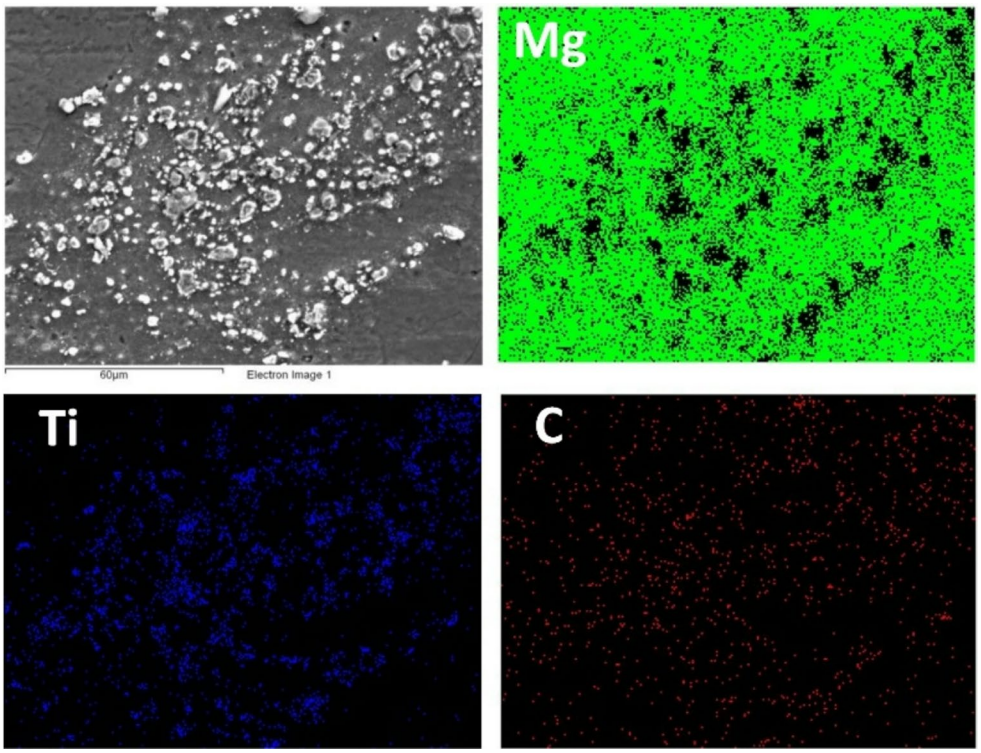

Fig. 3 Elements mapping of FSPd Mg-TiC showing existence of Mg, Ti and C

value from center of stirrer zone. Microhardness value of as stir cast Mg-TiC composite was 105 Hv whereas, microhardness value of the FSP 3 specimens was increased up to 133 Hv, which is almost 26% higher than as cast composite. FSP 1 also showed increased hardness as equated to as stir cast pure Mg, which have reached maximum up to 53 Hv.

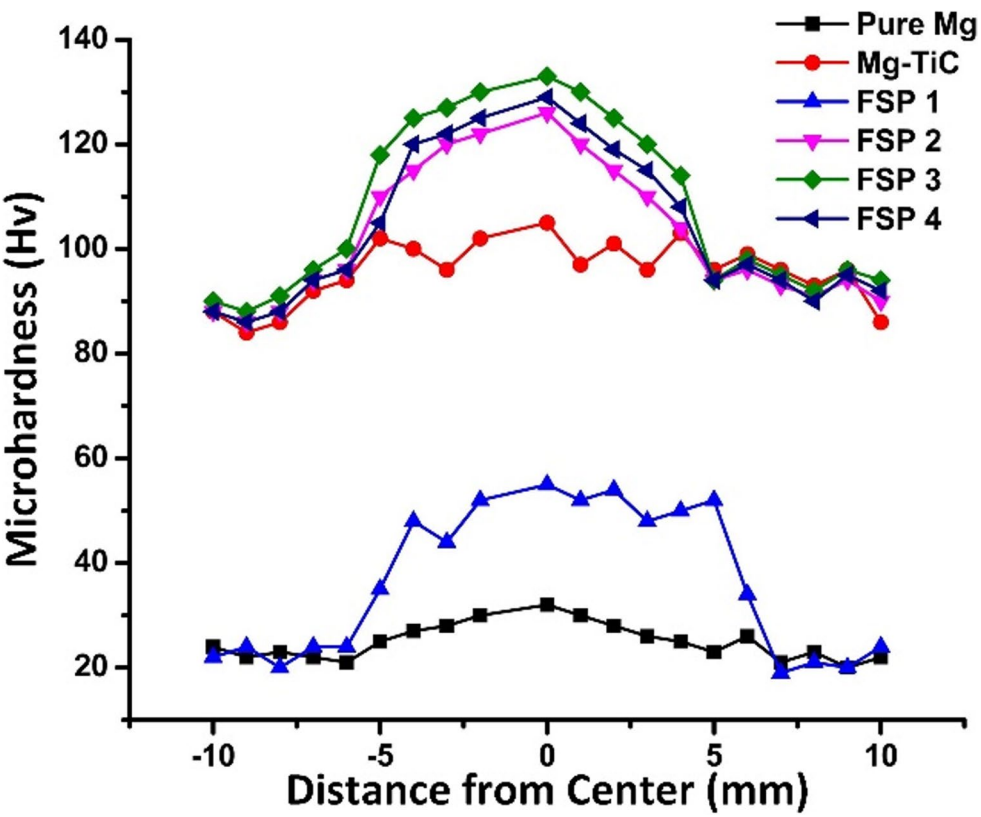

Fig. 4 Microhardness for cast and FSPd specimens

Table 1 Wear parameters and their levels

Factors	Parameters	Units	Levels				
			−2	−1	0	1	2
A	Load (P)	N	5	10	15	20	25
B	Sliding distance (S.D.)	m	250	500	750	1000	1250
C	Sliding velocity (S.V.)	m/s	0.25	0.5	0.75	1	1.25

Refined grain structure obtained during FSP results in the improved hardness. As per Hall-Petch equation as the grain size of particles reduced, hardness of material improved, and vice versa [41]. Microhardness of magnesium alloy (AM60) got enhanced by applying the FSP to alloy as compared to unprocessed alloy [42]. Ahmadkhaniha et al., observed enhanced microhardness for the FSPd magnesium as equated to the pure magnesium [20]. The inter-particle spacing decreases due to stirring action of tool, which increases hardness. So, it can be considered that reinforced particles along with FSP played noteworthy role for improving hardness of composite [43]. The enhanced hardness values of the FSPd (Mg-TiC) specimens could be accredited to the existence of uniformly distributed of reinforced particles as shown in Fig. 2(b). Stirring action of tool causes the plastic deformation [44], which refines the grains and reinforced TiC particles. The existence of refined TiC particles and refined microstructure improve the load carrying capacity that confines the deformation of the matrix material [45, 46]. The development of sub-grains, the uniform dispersion of TiC particles, and the existence of a significant fraction of high-angle grain boundaries in comparison to as-cast specimen all contribute to improvement in hardness [47].

Table 2 Experimental results for volumetric wear rate

Run Order	*P* (*N*)	S.D. (m)	S.V. (m/s)	Volumetric Wear Rate $\times 10^{-3}$
1	15	750	0.75	1.212
2	10	1000	1	1.268
3	10	1000	0.5	1.189
4	20	1000	0.5	1.385
5	15	750	0.25	1.185
6	15	750	0.75	1.245
7	20	500	1	1.325
8	15	750	0.75	1.259
9	10	500	1	1.253
10	15	750	1.25	1.299
11	20	1000	1	1.435
12	15	1250	0.75	1.444
13	15	750	0.75	1.289
14	15	750	0.75	1.256
15	15	750	0.75	1.272
16	5	750	0.75	1.155
17	20	500	0.5	1.296
18	25	750	0.75	1.493
19	10	500	0.5	1.201
20	15	250	0.75	1.235

3.3 Wear optimization

Table 1 shows the Wear parameters and their associated levels. Table 2 shows the 20 set of experiments based on CCD module in RSM. These experiments were performed by varying the P, S.D and S.V at five different levels. Volumetric wear rate has been considered as the output parameter and has been calculated from the equation mentioned below:

$$Volumetric\ Wear\ Rate = Loss\ in\ Weight\ (sliding\ distance) \tag{1}$$

A comprehensive model as shown in Eq. (2) is established to examine the effect of above mentioned wear parameters on volumetric wear rate.

$$\begin{gathered} Volumetric\ Wear\ Rate = +1.36964 \\ -0.016684\ P\ (N) - 0.000723\ S.D.(m) \\ +0.188318\ S.V.(m/s) + 0.000020\ P\ (N) * S.D.(m/s) \\ -0.005200\ P\ (N)\ * S.V.(m/s) + 0.000096 \\ S.V.(m/s)\ * S.D.(m)\ + 0.000699\ P\ (N) \\ * P\ (N) + 0.000000341455\ S.D.(m) * S.D.(m) \\ -\ 0.048545\ S.V.(m/s)\ *\ S.V.(m/s) \end{gathered} \tag{2}$$

ANOVA analysis using RSM was used to study the impact of input process parameters on volumetric wear rate. ANOVA study results of wear rate are displayed in Table 3. It has been concluded that the model is statistically noteworthy as the p-value is less than 0.05. Moreover, the lack of fit is inconsequential, which is desirable. At specified set of process parameters, wear rate models prove to be highly substantial and beneficial. The value of Adjusted R^2 is 90.72% and value of R^2 is 95.12%, which are very close to each other. This signifies that the model is significant.

The link between the residuals and the process parameters is clearly shown by the scatter diagrams in Fig. 5 (a–c), which also show how changes in P (N), S. D. (m) and S.V. (m/s) affect the wear rate. The normal probability plot of the residuals for volumetric wear rate is displayed in Fig. 6(a). It demonstrates that the errors are normally distributed as the residuals closely resemble a straight line. Figure 6 (b) displays the plot of actual versus predicted volumetric wear rate values, demonstrating an excellent fit between the regression model and the experimental data.

Table 3 ANOVA table for volumetric wear rate

Source	Sum of Squares	DF	Mean Square	F-value	*p*-value
Model	0.1508	9	0.0168	21.64	< 0.0001
P (N)	0.0352	1	0.0352	45.51	< 0.0001
S.D. (m)	0.0016	1	0.0016	2.01	0.1869
S.V. (m/s)	0.0056	1	0.0056	7.27	0.0225
P(N) × S.D. (m)	0.0048	1	0.0048	6.2	0.032
P (N) × S.V. (m/s)	0.0003	1	0.0003	0.4365	0.5238
S.D. (m) × S. V. (m/s)	0.0003	1	0.0003	0.3719	0.5556
P(N) × P(N)	0.0077	1	0.0077	9.9	0.0104
S.D. (m) × S.D. (m)	0.0115	1	0.0115	14.79	0.0032
S. V. (m/s) × S. V. (m/s)	0.0002	1	0.0002	0.2989	0.5966
Residual	0.0077	10	0.0008		
Lack of Fit	0.0043	5	0.0009	1.27	0.3993
Pure Error	0.0034	5	0.0007		
Cor Total	0.1586	19			

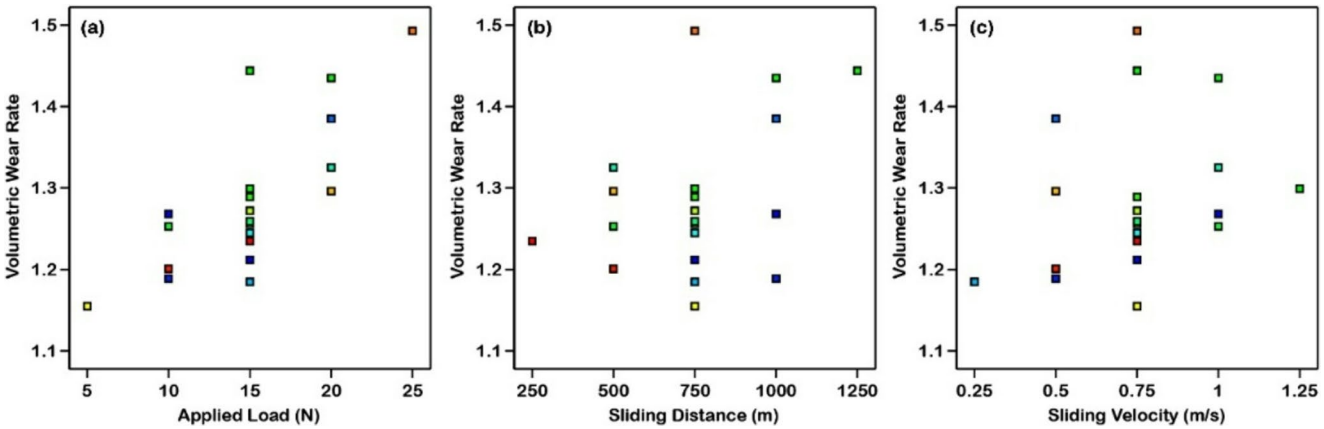

Fig. 5 Scatter Diagram of Volumetric Wear Rate versus (**a**) P (N) (**b**) S.D. (m) (**c**) Volumetric Wear Rate versus S.V. (m/s)

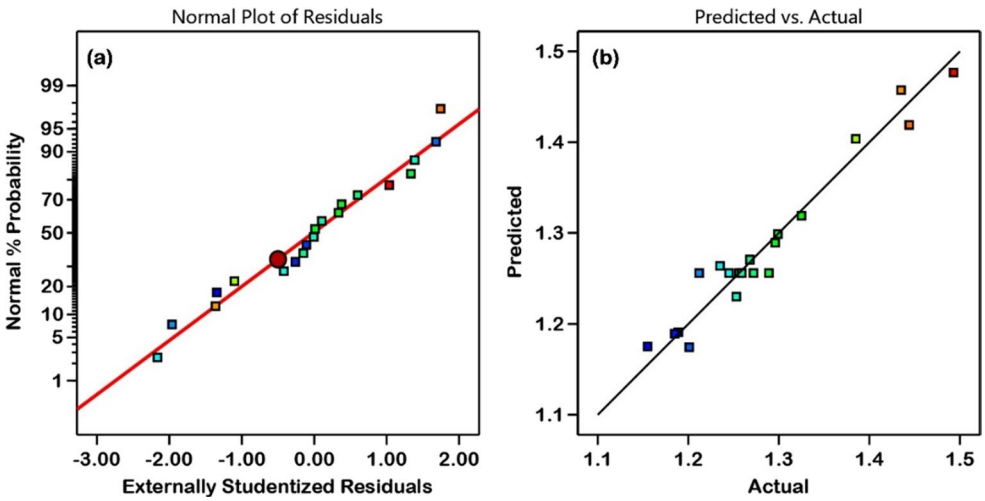

Fig. 6 Normal probability plot for volumetric wear rate (**a**) Residuals (**b**) Actual versus predicted

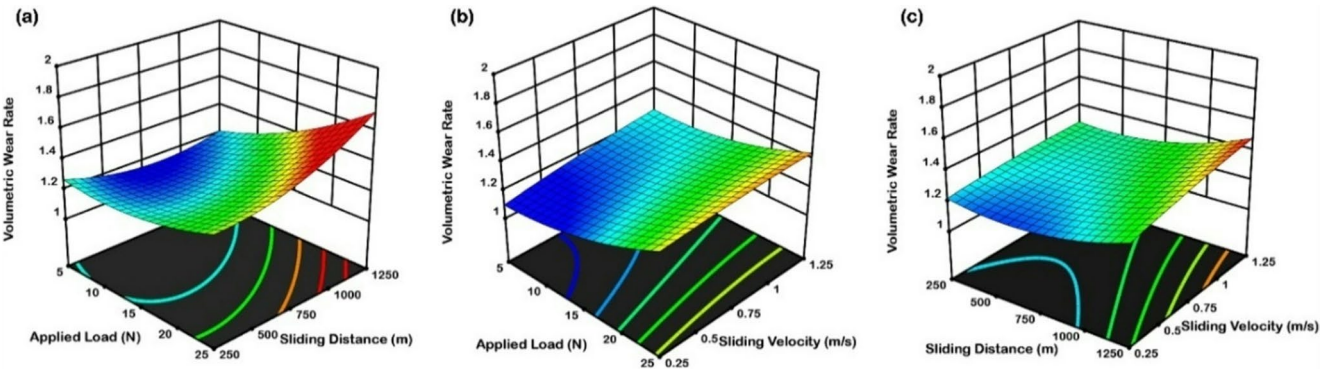

Fig. 7 3D surface plot for Volumetric Wear Rate (**a**) S.D. (m) vs. P (N), (**b**) S.V. (m/s) vs. Load P (N), (**c**) S.D. (m) vs. S.V. (m/s)

Figure 7 (a-c) shows the 3D surface plots for interaction effect of process parameters on volumetric wear rate. Figure 7 (a) depicts the effect of Sliding distance and applied load on volumetric wear rate. It has been concluded that the volumetric wear rate rises linearly with the increase in Sliding distance and applied load. With the increase in load and Sliding distance, temperature at the contact between the sample and counter plate rises which leads to a rise in volumetric wear rate for the FSP TiC workpiece. These results are in line with the results shown in [48, 49].

Figure 7 (b) displays the effect of P (N) and S. V. (m/s) on volumetric wear rate. It was observed that the increase in Sliding velocity causes slight decrease in volumetric wear rate. Similar results were reported by [50].

Figure 7 (c) relates the effect of sliding velocity and sliding distance on volumetric wear rate. It has been concluded that increase in sliding distance (250 to 1250 m), the volumetric wear rate shows a gradual overall rise. This indicates that prolonged sliding contributes to higher wear, likely due to the progressive degradation of material over time. On the other side, at lower velocities (0.25–0.5 m/s), the wear rate remains minimal. However, as the velocity increases (beyond 0.75 m/s), the volumetric wear rate significantly rises, particularly when paired with greater Sliding distances. This suggests a combined effect of higher velocity and extended Sliding distance on wear. These results are in good agreement with the results performed by kumar et al. [50].

An accuracy of the established model has been confirmed by conducting the confirmation test. In this, the experiments were conducted at several process parameter levels that were not included in the initial design. Table 4 presented the results of the confirmation test. Using Design of Experiments (DOE), the predicted and calculated wear values are compared to calculate the error percentage. The error percentage from the experiment falls within ±4%, demonstrating that the regression model effectively predicts the wear rate with high accuracy.

3.4 Wear mechanisms

SEM images of worn surfaces of FSPd pure Mg and FSPd Mg-TiC specimen are represented in Fig. 8. The worn surface of FSPd Mg at low load (5 N) represented in Fig. 8 (a), which shows lesser wear rate. The worn surface at 5 N load showed fine and smooth wear tracks which indicates slight abrasive wear, shallow grooves. however, surface appearance at 25 N load (Fig. 8 (b)) indicates that the extent of abrasion increased, grooves appeared in sliding direction and oxidation of surface also occurred. This wear mechanism at 25 N load, might be accredited to heat produced between specimen and counter face steel disc [51]. Wear rate of specimen increases, as applied load increases. Specimen becomes soft due to high temperature that resulted into decreased surface hardness and increased ductility of material. High heat produced at higher load results in to increase in material loss. Ploughing marks found on whole worn surface represents third body abrasive wear caused by matrix debris. Ploughing marks become wider in comparison to 5 N load, which specify higher wear rate [52]. Oxidized surface was also found on worn surface that might be accredited to high heat produced at 25 N load.

The worn surface of FSPd samples at 5 N load showed (Fig. 8 (a) and (c)) slight abrasive wear, oxide layer and

Table 4 Confirmation experiments

Run Order	*P* (*N*)	S.D. (m)	S.V. (m/s)	Projected Value	Calculated Value	Error (%)
1	10	750	0.75	1.246	1.287	3.29
2	15	1000	1	1.398	1.416	1.29
3	25	250	0.25	1.406	1.438	2.28

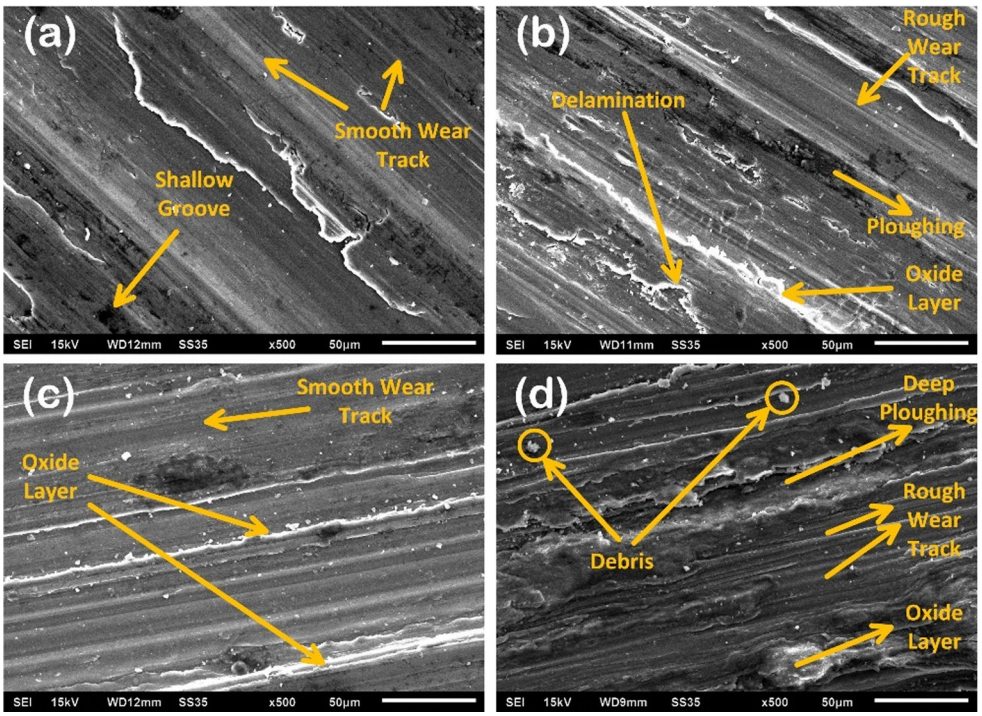

Fig. 8 SEM micrographs of worn surfaces (**a**) FSPd pure Mg at 5 N (**b**) FSPd pure Mg at 25 N (**c**) FSPd Mg-TiC at 5 N and (**d**) FSPd Mg-TiC at 25 N

smooth wear tracks, whereas worn surfaces at 25 N load showed (Fig. 8 (b) and (d)) the rough wear tracks, enhanced abrasion, ploughing and oxidation of specimen. Similar wear behavior was observed like abrasive marks, wear tracks on the FSPd surface of Al5083/B_4C composite [53]. Applied load is moved from matrix material to hard TiC particles, that acts as load carrying elements. The worn surface of FSPd specimen can be interrelated to enhancement in hardness, equal distribution of refined TiC particles attained after the FSP. The enhanced hardness confined the severe delamination and ploughing marks formed under varying load conditions, though its existence enhanced at higher load of 25 N. Ploughing marks are more prominent in Fig. 8 (d) due to existence of TiC particles which are pullouts at higher load and acts as third particle abrasion wear between specimen and steel disc. Friction stir processing composite specimens showed mild abrasion and oxidation mechanism.

Abrasive wear, which is caused by TiC particles and debris impacting the specimen surface, is one of the main wear mechanisms of the FSPd composite. Adhesive wear due to higher applied loads categorized as ploughing, delamination. Oxidative wear due to formation of oxide layers mainly occurred at higher load. Wear tracks can be seen prominently at higher load conditions. Abrasive wear is considered as main wear mechanism due to hard TiC particles present in the composite specimen act as abrasive component which removes material from specimen surface and steel disk during wear test. Debris produced during higher load conditions causes wear by ploughing. Ploughing marks clearly indicated in SEM of worn surfaces shown in Fig. 8 (b & d).

4 Conclusions

The TiC particle reinforced magnesium matrix composite fabricated by stir casting method. Cast Mg-TiC composite and cast pure Mg was processed by friction stir processing at three different rpm to enhance hardness and refine microstructure of cast specimens. Optimization technique (RSM) used to study the effects of parameters on wear behaviour of processed specimens. Wear mechanism was also study to analyze the wear pattern of worn specimens. The following were the key conclusions drawn from friction stir processed specimens:

- Microstructure and SEM images of FSPd specimens verified the refined microstructure and uniform dispersal of the TiC particles.
- As rotational speed increased the microhardness increased, but at 1600 rpm the hardness decreased. This may be due to excessive heat generated at 1600 rpm. Hence surface texture of FSP 4 becomes rough at 1600 rpm. So, FSP 4 specimen has lower hardness in comparison to FSP 3.
- The microhardness of FSP 3 was observed 26% higher than as cast Mg-TiC composite. Refined microstructure

and homogeneous dispersion of reinforcement particles leads to increased hardness.

- Outcome of RSM results reveal that volumetric wear rate showed increasing trend with respect to load, sliding distance and velocity. The applied regression model effectively forecasts the lowest wear rate, and a validation test confirms the error, which is within ±4%.
- SEM micrographs showed that as load increased (25 N) the wear tracks become rough and ploughing becomes deeper in comparison to 5 N load. Worn surfaces also showed oxide layer that produced due to heat generation during rubbing action between specimen and wear disk. Delamination and ploughing occurred at higher (25 N) load. Deep ploughing may be occurred due to third particles abrasion that occurred due to pullout reinforcement particle. Debris also observed at 25 N load for FSPd composite due to adhesive wear.

Acknowledgements The authors gratefully acknowledge Mr. Sukhwinder Singh, Plant Head of the Aspee Springs Limited, Baddi, India for facilitating FSP Machine and testing facility. The authors would like to acknowledge the funding from the Ongoing Research Funding Program, (ORF-2025-999), King Saud University, Riyadh, Saudi Arabia.

Authors contribution All authors equally contributed to the paper.

Data availability The data can be made available on a reasonable request to the corresponding author.

Declarations

Conflict of interest There is no conflict of interest.

References

1. S. Abazari, A. Shamsipur, H.R. Bakhsheshi-Rad, J.W. Drelich, J. Goldman, S. Sharif, A.F. Ismail, M. Razzaghi, Magnesium-based nanocomposites: a review from mechanical, creep and fatigue properties. J. Magnesium Alloy. **11**(8), 2655–2687 (2023). https://doi.org/10.1016/j.jma.2023.08.005
2. X. Wang, J. Liu, M. Huang, Y. Zheng, J. Yang, N. Li, X. Dong, A review on wear resistance of Mg alloys: the influence of common rare earth alloying elements and general modification techniques. Mater. Sci. Technol. (2024). https://doi.org/10.1177/02670836241262597
3. S. Shahid Ul Islam, N.Z. Khan, M.M. Khan, Effect of reinforcement on magnesium-based composites fabricated through stir casting: a review. Mater. Today Proc. **46**, 6513–6518 (2021). https://doi.org/10.1016/j.matpr.2021.03.710
4. M.A. Maleque, M. Radhi, M.M. Rahman, Wear study of Mg-SiCp reinforcement aluminium metal matrix composite. J. Mech. Eng. Sci. **10**(1), 1758–1764 (2016). https://doi.org/10.15282/jmes.10.1.2016.1.0169
5. A. Singh, N. Bala, Fabrication and tribological behavior of stir cast Mg/B_4C metal matrix composites. Metall. Mater. Trans. A **48**(10), 5031–5045 (2017). https://doi.org/10.1007/s11661-017-4203-x
6. S.D. Kumar, M. Ravichandran, M. Meignanamoorthy, S. Sakthivelu, S.V. Alagarsamy, C. Chanakyan, Investigations on properties of Mg-Al2O3 composites fabricated via stir casting route. Mater. Today Proc. **27**, 1132–1136 (2020). https://doi.org/10.1016/j.matpr.2020.01.586
7. Y. Mazaheri, M.M. Jalilvand, A. Heidarpour, A.R. Jahani, Tribological behavior of AZ31/ZrO_2 surface nanocomposites developed by friction stir processing. Tribol Int. **143**, 106062 (2020). https://doi.org/10.1016/j.triboint.2019.106062
8. A. Ramanathan, P.K. Krishnan, R. Muraliraja, A review on the production of metal matrix composites through stir casting – furnace design, properties, challenges, and research opportunities. J. Manuf. Process. **42**, 213–245 (2019). https://doi.org/10.1016/j.jmapro.2019.04.017
9. G.S. Arora, K.K. Saxena, K.A. Mohammed, C. Prakash, S. Dixit, Manufacturing techniques for Mg-based metal matrix composite with different reinforcements. Crystals **12**(7), 945 (2022). https://doi.org/10.3390/cryst12070945
10. B. Gugulothu, P. Anusha, M.N. Swapna Sri, S. Vijayakumar, R. Periyasamy, S. Seetharaman, Optimization of stir-squeeze casting parameters to analyze the mechanical properties of Al7475/B4C/Al2O3/TiB2 hybrid composites by the Taguchi method. Adv. Mater. Sci. Eng. **2022**, 1–9 (2022). https://doi.org/10.1155/2022/3180442
11. M.T. Sijo, K.R. Jayadevan, Analysis of stir cast aluminium silicon carbide metal matrix composite: a comprehensive review. Procedia Technol. **24**, 379–385 (2016). https://doi.org/10.1016/j.protcy.2016.05.052
12. B. Ram, D. Deepak, N. Bala, Role of friction stir processing in improving wear behavior of mg/sic composites produced by stir casting route. Mater. Res. Express (2018). https://doi.org/10.1088/2053-1591/aaf1e4
13. V. Sharma, U. Prakash, B.V.M. Kumar, Surface composites by friction stir processing: a review. J. Mater. Process. Technol. **224**, 117–134 (Oct. 2015). https://doi.org/10.1016/j.jmatprotec.2015.04.019
14. C. Zhu, Y. Lv, C. Qian, Q. Chao, J. Haixin, W. Ting, Z. Liqiang, F. Zhang, Proliferation and osteogenic differentiation of rat BMSCs on a novel ti/sic metal matrix nanocomposite modified by friction stir processing. Sci. Rep. **6**(1), 38875 (2016). https://doi.org/10.1038/srep38875
15. R. Kumar, H. Kumar, S. Kumar, J.S. Chohan, Effects of tool pin profile on the formation of friction stir processing zone in AA1100 aluminium alloy. Mater. Today Proc. **48**, 1594–1603 (2022). https://doi.org/10.1016/j.matpr.2021.09.491
16. A.P. Zykova, S.Y. Tarasov, A.V. Chumaevskiy, E.A. Kolubaev, A review of friction stir processing of structural metallic materials: process, properties, and methods. Metals **10**(6), 772 (2020). https://doi.org/10.3390/met10060772
17. S.A. Manroo, N.Z. Khan, B. Ahmad, Study on surface modification and fabrication of surface composites of magnesium alloys

by friction stir processing: a review. J. Eng. Appl. Sci. **69**(1), 25 (2022). https://doi.org/10.1186/s44147-022-00073-9
18. J. Iwaszko, K. Kudła, Microstructure, hardness, and wear resistance of AZ91 magnesium alloy produced by friction stir processing with air-cooling. Int. J. Adv. Manuf. Technol. **116**(3–4), 1309–1323 (2021). https://doi.org/10.1007/s00170-021-07474-9
19. R. Koganti, A.K. Lakshminarayanan, T. Ramprabhu, Understanding the effect of tool rotational speed on microstructure and mechanical properties of friction stir processed ZE41 grade magnesium alloy. 427–435 (2019). https://doi.org/10.1007/978-981-13-1780-4_41
20. D. Ahmadkhaniha, M. Heydarzadeh Sohi, A. Salehi, R. Tahavvori, Formations of AZ91/Al_2O_3 nano-composite layer by friction stir processing. J. Magnesium Alloys **4**(4), 314–318 (2016). https://doi.org/10.1016/j.jma.2016.11.002
21. J. Shang, L. Ke, F. Liu, F. Lv, L. Xing, Aging behavior of nano SiC particles reinforced AZ91D composite fabricated via friction stir processing. J. Alloys Compd. **797**, 1240–1248 (2019). https://doi.org/10.1016/j.jallcom.2019.04.280
22. V. Chaudhary, R. Verma, V. Sharma, Effect of nanoparticles adhesion and multipass friction stir processing on metallurgical properties of AZ91D magnesium alloy. J. Adhes. Sci. Technol. **38**(11), 1953–1973 (2024). https://doi.org/10.1080/01694243.2023.2282828
23. G. Rajan, A. kumar, A.K. Godasu, S. Mula, Effect of friction stir processing on microstructural evolution and mechanical properties of nanosized SiC reinforced AA5083 nanocomposites developed by stir casting. Mater. Today Commun. **35**, 105912 (2023). https://doi.org/10.1016/j.mtcomm.2023.105912
24. V. Sharma, Y. Gupta, B.V.M. Kumar, U. Prakash, Friction stir processing strategies for uniform distribution of reinforcement in a surface composite. Mater. Manuf. Process. **31**(10), 1384–1392 (2016). https://doi.org/10.1080/10426914.2015.1103869
25. C.J. Singh, B. Ram, J. Singh, C. Prakash, P. Paramasivam, R. Kumar, Experimental investigation on characterization of friction stir processed AZ31-based composite. Sci. Rep. **14**(1), 15453 (2024). https://doi.org/10.1038/s41598-024-66379-1
26. J. Hu, K. Yang, Q. Wang, Q.C. Zhao, Y.H. Jiang, Y.J. Liu, Ultralong life fatigue behavior of a high-entropy alloy. Int. J. Fatigue. **178**, 108013 (2024). https://doi.org/10.1016/j.ijfatigue.2023.108013
27. S. Gajević, S. Miladinović, B. Stojanović, Metallic nanocomposites: an introduction,Nanotechnology in the Automotive Industry. Elsevier. 155–161 (2022). https://doi.org/10.1016/B978-0-323-90524-4.00008-6
28. M. Navazani, K. Dehghani, Investigation of microstructure and hardness of mg/tic surface composite fabricated by friction stir processing (FSP). Procedia Mater. Sci. **11**, 509–514 (2015). https://doi.org/10.1016/j.mspro.2015.11.082
29. M. Balakrishnan, I. Dinaharan, R. Palanivel, R. Sivaprakasam, Synthesize of AZ31/TiC magnesium matrix composites using friction stir processing. J. Magnes. Alloy. **3**(1), 76–78 (2015). https://doi.org/10.1016/j.jma.2014.12.007
30. B. Singh, J. Singh, R.S. Joshi, Effect of tic reinforcement on wear resistance of magnesium matrix composite by FSP. Arch. Metall. Mater. 293–302 (2021). https://doi.org/10.24425/amm.2022.137505
31. K. Kalita, I. Shivakoti, R.K. Ghadai, Optimizing process parameters for laser beam micro-marking using genetic algorithm and particle swarm optimization. Mater. Manuf. Process. **32**(10), 1101–1108 (2017). https://doi.org/10.1080/10426914.2017.1303156
32. K. Kalita, V. Kumar, S. Chakraborty, A novel MOALO-MODA ensemble approach for Multi-objective optimization of machining parameters for metal matrix composites. Aug. **02** (2022). https://doi.org/10.21203/rs.3.rs-1896308/v1
33. S. Mohal, S. Chaitanya, M. Singh, R. Goyal, A. Kumar, G. Saini, Analyzing the response of submerged arc welding process parameters on form factor and dilution. Mater. Today Proc. **56**, 2556–2562 (2022). https://doi.org/10.1016/j.matpr.2021.09.143
34. S. Kumar, S. Kumar, R. Mehra, Parametric evaluation of PMEDM for the machining of inconel-800 using response surface methodology. Mater Today Proc Feb. (2023). https://doi.org/10.1016/j.matpr.2023.02.048
35. R. Mehra, S. Mohal, B. Lonia, M. Kumar, Optimization of laser engraving process parameters for the engraving of hybrid glass fiber reinforced plastic (GFRP) combinations. Lasers Eng. **45**, 265–281 (2020)
36. A. Singh, N. Bala, Relative sliding wear behavior of Mg metal matrix composites fabricated by stir cast route, Mater Res Express. **6**(10), 1065h1 (2019). https://doi.org/10.1088/2053-1591/ab4313
37. A. Shiva, M. Cheepu, V.C. Kantumuchu, K.R. Kumar, D. Venkateswarlu, B. Srinivas, Jerome microstructure characterization of Al-TiC surface composite fabricated by friction stir processing. IOP Conf. Ser. Mater. Sci. Eng. **330**, 012060 (2018). https://doi.org/10.1088/1757-899X/330/1/012060
38. M.R. Akbarpour, H.M. Mirabad, F. Gazani, I. Khezri, A.A. Chadegani, A. Moeini, H.S. Kim, An overview of friction stir processing of Cu–SiC composites: microstructural, mechanical, tribological, and electrical properties. J. Mater. Res. Technol. **27**, 1317–1349 (2023). https://doi.org/10.1016/j.jmrt.2023.09.200
39. H.B.M. Rajan, I. Dinaharan, S. Ramabalan, E.T. Akinlabi, Influence of friction stir processing on microstructure and properties of AA7075/TiB 2 in situ composite. J. Alloys Compd. **657**, 250–260 (2016). https://doi.org/10.1016/j.jallcom.2015.10.108
40. K. Patel, N.D. Ghetiya, S. Bharti, Effect of single and double pass friction stir processing on microhardness and wear properties of AA5083/Al2O3 surface composites. Mater. Today Proc. **57**, 38–43 (2022). https://doi.org/10.1016/j.matpr.2022.01.256
41. A.Z. Naser, B.M. Darras, Experimental investigation of mg/sic composite fabrication via friction stir processing. Int. J. Adv. Manuf. Technol. **91**, 1–4 (2017). https://doi.org/10.1007/s00170-016-9801-z
42. J. Iwaszko, K. Kudła, K. Fila, M. Strzelecka, The effect of friction stir processing (FSP) on the microstructure and properties of AM60 magnesium alloy. Arch. Metall. Mater. **61**(3), 1555–1560 (2016). https://doi.org/10.1515/amm-2016-0254
43. S. Jayalakshmi, R. Arvind Singh, T.S. Srivatsan, Effect of matrix properties and sliding counterface on the wear behavior of magnesium alloy metal matrix composites. 135–148 (2018). https://doi.org/10.1007/978-3-319-72853-7_10
44. H. Mirzadeh, High strain rate superplasticity via friction stir processing (FSP): a review. Mater. Sci. Eng.: A. **819**, 141499 (2021). https://doi.org/10.1016/j.msea.2021.141499
45. S. Aravindan, P.V. Rao, K. Ponappa, Evaluation of physical and mechanical properties of AZ91D/SiC composites by two step stir casting process. J. Magnesium Alloys **3**(1), 52–62 (2015). https://doi.org/10.1016/j.jma.2014.12.008
46. D. Kumar, L. Thakur, A study of development and sliding wear behavior of AZ91D/Al_2O_3 composites fabricated by ultrasonic-assisted stir casting. Arab. J. Sci. Eng. **48**(3), 2951–2967 (2023). https://doi.org/10.1007/s13369-022-07032-9
47. M. Al-Saadi, F. Sandberg, C. Hulme-Smith, A. Karasev, P.G. Jönsson, A study of the static recrystallization behaviour of cast alloy 825 after hot-compressions. J. Phys. Conf. Ser. **1270**(1),

012023 (2019). https://doi.org/10.1088/1742-6596/1270/1/012023

48. P. Han, J. Lin, W. Wang, Z. Liu, Y. Xiang, T. Zhang, Q. Liu, X. Guan, K. Qiao, Y. Xie, K. Wang, Friction stir processing of cold-sprayed high-entropy alloy particles reinforced aluminum matrix composites: corrosion and wear properties. Met. Mater. Int. **29**(3), 845–860 (2023). https://doi.org/10.1007/s12540-022-01248-y
49. H.R. Lashgari, S. Zangeneh, Particle-stimulated nucleation (PSN) in the Co–28Cr–5Mo–0.3 C alloy. Metals **10**(5), 671 (2020). https://doi.org/10.3390/met10050671
50. T.S. Kumar, R. Raghu, G.S. Priyadharshini, R. Čep, K. Kalita, A study on microstructural, mechanical properties, and optimization of wear behaviour of friction stir processed AZ31/TiC composites using response surface methodology. Sci. Rep. (2024). https://doi.org/10.1038/s41598-024-69348-w
51. K. Soorya Prakash, P. Balasundar, S. Nagaraja, P.M. Gopal, V. Kavimani, Mechanical and wear behaviour of Mg–SiC–Gr hybrid composites. J. Magnesium Alloys **4**(3), 197–206 (2016). https://doi.org/10.1016/j.jma.2016.08.001
52. F. Aydın, Tribological aspects of magnesium matrix composites: a review of recent experimental studies. Tribology - Materials, Surfaces & Interfaces **17**(4), 363–396 (2023). https://doi.org/10.1080/17515831.2023.2246809
53. N. Yuvaraj, S. Aravindan, Vipin, Fabrication of Al5083/B_4C surface composite by friction stir processing and its tribological characterization. J. Mater. Res. Technol. **4**(4), 398–410 (2015). https://doi.org/10.1016/j.jmrt.2015.02.006